Enhancement of Second-Harmonic Generation from Metal Nanoparticles by Passive Elements

Robert Czaplicki,* Hannu Husu,† Roope Siikanen, Jouni Mäkitalo, and Martti Kauranen
Optics Laboratory, Department of Physics, Tampere University of Technology, P.O. Box 692, FI-33101 Tampere, Finland

Janne Laukkanen, Joonas Lehtolahti, and Markku Kuittinen
Department of Physics and Mathematics, University of Eastern Finland, FI-80101 Joensuu, Finland
(Received 9 October 2012; published 28 February 2013)

We prepare arrays of gold nanoparticles that include both noncentrosymmetric particles with a second-order nonlinear optical response (active particles) and centrosymmetric particles with no second-order response (passive particles). The plasmon resonances of the active and passive particles are at distinct wavelengths, yet the passive particles modify the electromagnetic modes of the structure in such a way that second-harmonic generation from the active particles is enhanced. Our results provide a completely new concept for optimizing the nonlinear responses of metamaterials.

DOI: 10.1103/PhysRevLett.110.093902 PACS numbers: 42.65.Ky, 42.65.−k, 78.67.Bf

The optical properties of metal nanoparticles arise from their localized surface plasmon resonances, which depend sensitively on the particle size and shape as well as the surrounding material [1]. Such particles are often used as basic units for metamaterials, which can possess optical properties not encountered in naturally occurring materials [2,3]. The metamaterials often consist of arrays of identical particles, where the overall response is determined by the resonances of the individual particles and their mutual electromagnetic coupling [4–6]. This provides several degrees of freedom for the design and fabrication of structures with enhanced optical responses.

Optical antennas are a specific concept made possible by properly designed metal nanoparticles [7–11]. They enable coupling of optical radiation from the near field of a radiation source to the far field [7,10,12] or vice versa. Such effects can be interpreted as a modification of the electromagnetic environment near the source or the receiver. Passive elements play an important role in the design of antennas [13,14]. They are used to improve the directionality or other properties of the antennas, which can also be interpreted as a further modification in the electromagnetic structure of space.

In order to have a second-order nonlinear optical response, the nanostructures need to be noncentrosymmetric. More specifically, the structure should appear noncentrosymmetric even at normal incidence, because experiments performed at oblique angle of incidence provide coupling with the traditional surface nonlinearity that exists for any material. Common second-order structures have therefore consisted of L-shaped or T-shaped particles [15–17] or dimers [18] and split-ring resonators [15,19,20]. Recent improvements in sample quality have led to structures that fulfill the polarization selection rules for the second-order response very well [21,22].

It is now well established that a plasmonic resonance at the fundamental frequency and its quality are beneficial for second-harmonic generation (SHG) [15,19,23] and third-harmonic generation [24,25]. A resonance at the harmonic frequency, on the other hand, is seen as a loss mechanism [23], in contrast to how resonant nanoantennas are utilized to enhance outcoupling from other types of sources [13]. The quality of the resonance also plays an important role in the nonlinear efficiency [21], which can be tailored through photonic resonances of the arrays [6,26]. The nonlinear response also depends on particle density, but attempts to increase the density of split-ring resonators have led to broadened plasmon lines, which limits the achievable efficiency [24,27]. It is therefore evident that other types of approaches need to be considered to enhance the conversion efficiency.

In this Letter, we demonstrate a new concept where SHG from an array of L-shaped noncentrosymmetric particles is enhanced by the use of passive elements, which are centrosymmetric nanobars. The passive elements do not produce SHG as such, but they modify the plasmon resonances and the local electromagnetic fields of the L particles in such a way that the SHG efficiency is enhanced. This occurs in spite of the fact that the plasmon resonances of the active and passive particles are at very different wavelengths. By investigating a series of different samples, we confirm that in the present case the passive particles affect the plasmon resonances and local fields at the fundamental frequency. The results can be understood in terms of the coupling of the active and passive particles through lattice interaction, and they provide completely new opportunities for optimizing the nonlinear responses of metamaterials.

Our samples were fabricated by the standard electron-beam lithography and lift-off techniques. All sample designs were fabricated on the same fused silica substrate. In the vertical direction, the 0.5 mm thick fused silica substrate was coated with a 3 nm chromium adhesion layer followed by 20 nm of gold and a 20 nm protective layer of

silica. In the sample plane, all particles were ordered in an underlying two-dimensional square lattice with 500 nm period in x and y directions (Fig. 1). The reference samples consisted of only L's in an array of 1000 nm period [Figs. 1(a) and 1(b)].

The L-shaped SHG-active particles are strongly dichroic with plasmon resonances at distinct wavelengths for light polarized along the symmetry axis (y) and orthogonal to that (x) [28]. For the present work, the particles were designed to have either x- or y-polarized resonance near 1060 nm, which is the fundamental laser wavelength used in the SHG experiments. This was achieved by the linewidth of 100 nm and arm length of 175 nm (x resonance) and 275 nm (y resonance). The passive bars had a 50 nm linewidth and 300 nm length. The designs and SEM images of the samples are shown in Fig. 1.

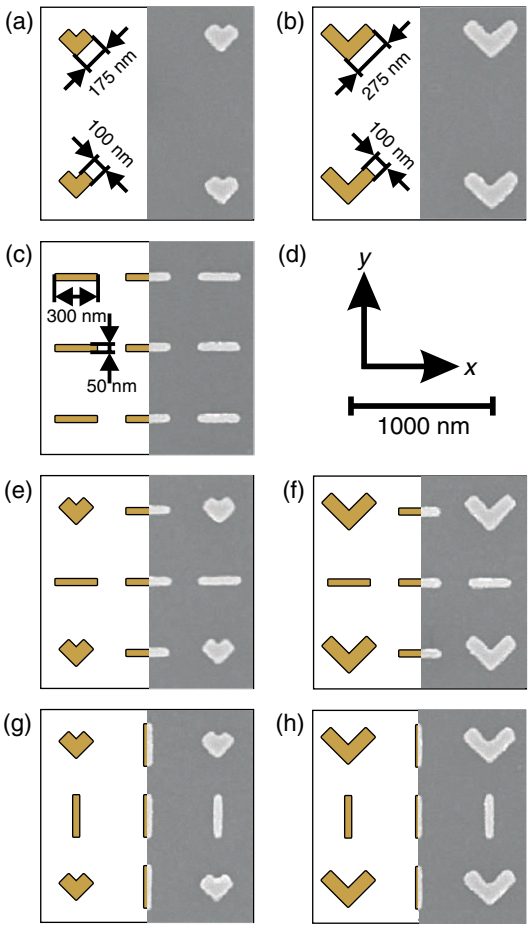

FIG. 1 (color online). Designs and SEM pictures of the samples. (a) Sample 175L, active L's with 175 nm arm length; (b) sample 275L, active L's with 275 nm arm length; (c) sample bar, passive bars with 300 nm length; (d) the coordinate system for the samples and scale bar; (e) sample 175L_xbar, active L's with 175 nm arm length and passive bars in x orientation; (f) sample 275L_xbar, active L's with 275 nm arm length and passive bars in x orientation; (g) sample 175L_ybar, active L's with 175 nm arm length and passive bars in y orientation; (h) sample 275L_ybar, active L's with 275 nm arm length and passive bars in y orientation.

Our SHG-active reference samples consisted of only L particles in a square array of 1000 nm period [Figs. 1(a) and 1(b)]. The passive reference samples consisted of only bars at each lattice point [Fig. 1(c)]. Finally, the samples combining L's and bars included the L's in the original positions, whereas the bars were placed in the remaining lattice points and they were oriented either along the x [Figs. 1(e) and 1(f)] or y direction [Figs. 1(g) and 1(h)].

The linear response of the samples was verified by measuring their extinction spectra at normal incidence. A halogen bulb was used as a broadband light source, which was fiber coupled to the measurement setup. The light from the fiber output was collimated using a microscope objective and a pinhole in front of the sample was used to illuminate only the desired sample area. The light after the sample was focused to a fiber connected to a spectrometer for recording the spectra. Indeed, two spectrometers were used to cover a spectral range from 400 to 1700 nm. The measurements were performed for both x- and y-polarized light. The results shown in Fig. 2 confirm that the small L's (175L) do have x- and y-polarized resonances at 1040 and 820 nm, respectively, whereas these resonances for the large L's (275L) are at 1670 and 1070 nm. The bars (bar), on the other hand, have longitudinal and transverse plasmon resonances at the 1470 and 555 nm wavelengths, respectively. Note that the resonances of the bars are at very different wavelength than

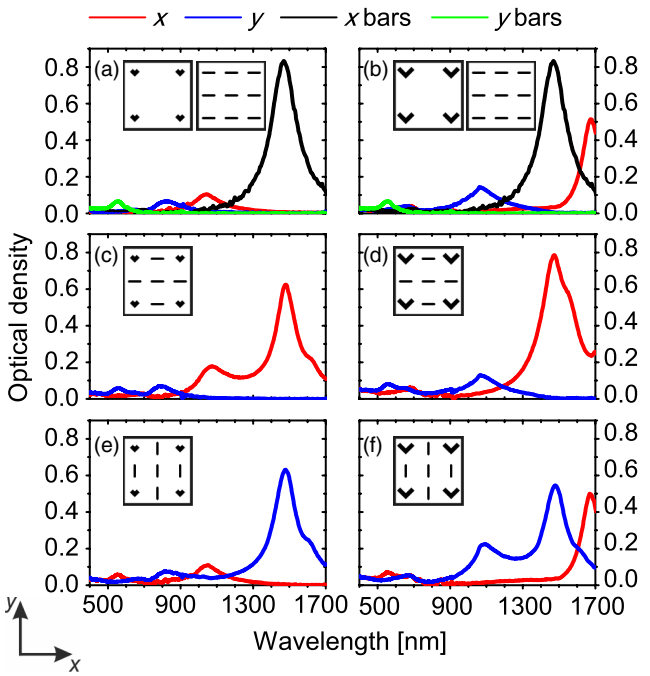

FIG. 2 (color online). Polarized extinction spectra of samples: (a) 175L and bar, (b) 275L and bar, (c) 175L_xbar, (d) 275L_xbar, (e) 175L_ybar, and (f) 275L_ybar.

any of the L resonances and, most importantly, the fundamental laser wavelength.

The results for the samples combining the two types of particles, however, show that the bars modify the resonances of the L's more than a mere superposition of the L and bar spectra. In particular, the bars are shown to enhance the plasmon peak at the laser wavelength by about a factor of 2 whenever the long axis of the bars is oriented along the polarization of this resonance. This suggests that the two types of particles are coupled in spite of the fact that their resonances occur at different wavelengths. When the bars are oriented orthogonally to polarization matching resonance at the laser wavelength, the plasmon peak at the fundamental wavelength remains almost unchanged.

The SHG measurements were performed using a Nd:glass laser (1060 nm, 200 fs, 200 mW, 82 MHz) as the source of fundamental light (Fig. 3). The laser beam was weakly focused with a 30 cm focal length lens to a spot size of about 300 μm at the sample, allowing the results to be analyzed in the plane wave limit. The beam was applied at normal incidence and its linear polarization was controlled by a calcite Glan polarizer and half-wave plate. The detected SHG polarization was selected by a Glan polarizer acting as an analyzer. A visible blocking filter was placed before the sample to filter out second-harmonic signal from the polarization optics and an infrared blocking filter was placed after the sample to block the fundamental laser beam. The second-order response was obtained by determining the quadratic dependence of the SHG intensity on the fundamental input intensity. The SHG was measured with a photomultiplier tube combined with a photon counting unit for sensitive light detection.

The symmetry of the sample dictates that the nonvanishing SHG signals correspond to the tensor components yyy and yxx, where the first letter refers to the polarization component of SHG light and the two latter letters refer to the polarization of the fundamental field. The symmetry also allows the tensor components $xxy = xyx$, but these components cannot be addressed individually. We will therefore focus on the components yyy and yxx, which are expected to be most strongly affected by the fundamental resonance.

The SHG signal levels of the samples are shown in Fig. 4. The reference samples (175L and 275L) have the strongest SHG signal for the tensor component for which the polarization of the fundamental wavelength is resonant with the particle (yxx for 175L and yyy for 275L). The SHG from bars was very close to the level of the background noise, as should be based on their centrosymmetry and in agreement with them being passive elements.

Combining active L nanoparticles with passive elements results in enhancement of SHG signals for properly designed samples (175L_xbar and 275L_ybar). The enhancement of tensor component yxx is observed for the sample 175L_xbar, for which the bars are oriented in the x direction, which is the resonant polarization of the L particles. Similar behavior is seen in the case of sample 275L_ybar, where the enhanced tensor component is yyy, which matches the orientation of passive elements with the y-polarized resonance of active particles. The enhancement for both cases is about a factor of 2 compared to the respective reference samples (175L and 275L).

The enhancements are closely related to the linear response of the samples (Fig. 2), where samples 175L_xbar and 275L_ybar show significant increase in the optical density at the laser wavelength due to the presence of bars. Such a result suggests that the enhancement in the SHG response is related to the modification of the plasmon resonances at the fundamental wavelength by the passive elements and the associated local-field distributions. Furthermore, the SHG signals from samples 175L_ybar and 275L_xbar, which consist of active and passive elements with bars oriented in the orthogonal direction compared to samples 175L_xbar and 275L_ybar, are modified very little by the bars and the modification can be either up or down (Fig. 4).

The results can be explained qualitatively through the coupled dipole model [29]. In this method, each particle at position $\mathbf{r}_n$ in the array is treated as a point electric dipole with a polarizability tensor $\vec{\alpha}_n$. Denote the electric field at $\mathbf{r}_n$ by $\mathbf{E}_n$. The dipole moment is then $\mathbf{p}_n = \epsilon_0 \vec{\alpha}_n \mathbf{E}_n$, where ϵ_0 is the permittivity of the vacuum. The local electric field

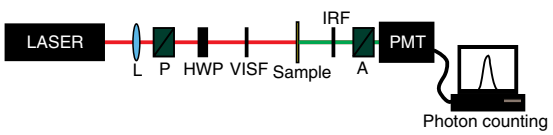

FIG. 3 (color online). Experimental setup for second-harmonic measurements. L, lens; P, Glan polarizer; HWP, half-wave plate; VISF, visible blocking filter; IRF, infrared blocking filter; A, analyzer; PMT, photomultiplier tube.

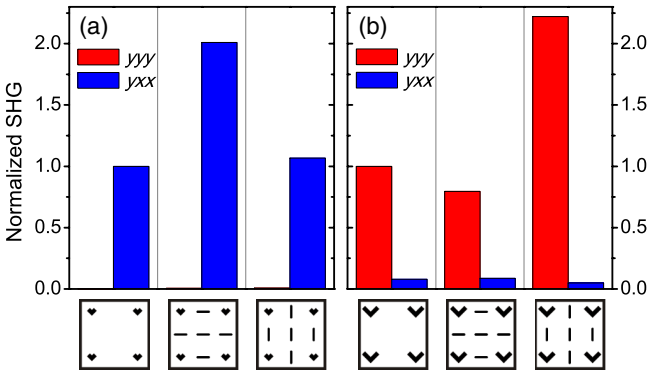

FIG. 4 (color online). SHG signals from the samples normalized to the stronger signal of L nanoparticles (yxx for 175L and yyy for 275L). (a) L's with 175 nm arm length (175L, 175L_xbar, and 175L_ybar). The signals yyy are much weaker than yxx (less than 0.01) and thus are not visible on the graph. (b) L's with 275 nm arm length (275L, 275L_xbar, and 275L_ybar).

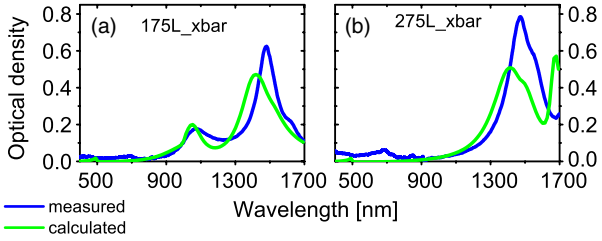

FIG. 5 (color online). Experimental [x polarization, cf. Figs. 2(c) and 2(d); measured, blue curve] and calculated (green curve) from the coupled dipole model optical density spectra for the samples (a) 175L_xbar and (b) 275L_xbar.

polarizing the dipole in the array is the superposition of the incident electric field $\mathbf{E}_0$ and the electric field scattered by the other dipoles in the array, which can be expressed as

$$\mathbf{E}_m = \mathbf{E}_{0m} + k^2 \sum_{n \neq m} \vec{G}(\mathbf{r_m}, \mathbf{r_n}) \vec{\alpha}_n \mathbf{E}_n, \qquad (1)$$

where $\vec{G}(\mathbf{r}, \mathbf{r}') = (\mathbf{I} + k^{-2}\nabla\nabla)\exp(ikR)/(4\pi R)$ is Green's tensor, $R = |\mathbf{r} - \mathbf{r}'|$, k is the wave number, and m, n run over all the particles in the sample. We apply this model to our case of four particles in the unit cell and two distinct polarizabilities (one for a bar and one for an L). We first obtain the complex polarizabilities of the L's and bars by fitting a Lorentzian to the measured spectra in Figs. 2(a) and 2(b). The spectra predicted by our model for 175L_xbar and 275L_xbar are shown in Fig. 5 (see Supplemental Material [30] for details). These spectra thus take into account the interactions between the dipoles through the lattice, and their qualitative agreement with the experimental spectra is very good. We also calculated the spectra for the remaining polarizations and samples (not shown). For all cases, we observed similar agreement. The differences between the spectral positions in the experimental and theoretical results are mainly due to the fact that we used the simplest possible form of Green's function, which does not fully account for the substrate and interfaces of the real sample.

The present results thus exhibit a clear enhancement of the SHG signals by appropriately oriented passive elements, but the enhancement factor of 2 is relatively modest. We emphasize, however, that there is plenty of room for further optimization of the basic concept. The enhancement here was achieved by passive elements that are essentially nonresonant. Larger enhancement can be expected from resonant elements. In addition, the passive elements were located far from the active particles. Optimizing the relative locations of the two types of particles could further improve the enhancement. Finally, the present results rely on affecting the plasmon resonances only at the fundamental wavelength. Additional enhancement can be expected by utilizing elements that enhance the outcoupling of SHG radiation. However, this will require careful sample design in order to optimize the spatial overlap of the plasmonic modes at the fundamental and SHG wavelengths.

In conclusion, we have shown that the efficiency of SHG from noncentrosymmetric metal nanoparticles can be enhanced by adding centrosymmetric passive elements in the sample design. This novel concept was demonstrated for the case where the passive elements modify the plasmon resonances of the active particles at the fundamental wavelength. A factor of 2 enhancement was observed, although the passive elements were nonresonant. We believe that this basic concept can be further optimized for simultaneous enhancement of the fundamental and SHG modes and therefore provides completely new opportunities for the design on nonlinear metamaterials.

This work was supported by the Academy of Finland (132438). H. H. and J. M. acknowledge the Graduate School of Tampere University of Technology for financial support. The authors would like to thank Kalle Koskinen for experimental assistance.

*robert.czaplicki@tut.fi
†Also at Centre for Metrology and Accreditation (MIKES), P.O. Box 9, FI-02151 Espoo, Finland.

[1] K. Kelly, E. Coronado, L. Zhao, and G. Schatz, J. Phys. Chem. B **107**, 668 (2003).
[2] V. M. Shalaev, Nat. Photonics **1**, 41 (2007).
[3] C. M. Soukoulis and M. Wegener, Nat. Photonics **5**, 523 (2011).
[4] Y. Chu, E. Schonbrun, T. Yang, and K. B. Crozier, Appl. Phys. Lett. **93**, 181108 (2008).
[5] B. Auguié and W. L. Barnes, Phys. Rev. Lett. **101**, 143902 (2008).
[6] K. D. Ko, A. Kumar, K. H. Fung, R. Ambekar, G. L. Liu, N. X. Fang, and K. C. Toussaint, Nano Lett. **11**, 61 (2011).
[7] P. Mühlschlegel, H.-J. Eisler, O. J. F. Martin, B. Hecht, and D. W. Pohl, Science **308**, 1607 (2005).
[8] J.-J. Greffet, Science **308**, 1561 (2005).
[9] P. Bharadwaj, B. Deutsch, and L. Novotny, Adv. Opt. Photonics **1**, 438 (2009).
[10] L. Novotny and N. van Hulst, Nat. Photonics **5**, 83 (2011).
[11] P. Biagioni, J.-S. Huang, and B. Hecht, Rep. Prog. Phys. **75**, 024402 (2012).
[12] T. Kosako, Y. Kadoya, and H. F. Hofmann, Nat. Photonics **4**, 312 (2010).
[13] T. H. Taminiau, F. D. Stefani, and N. F. van Hulst, Opt. Express **16**, 10 858 (2008).
[14] A. G. Curto, G. Volpe, T. H. Taminiau, M. P. Kreuzer, R. Quidant, and N. F. van Hulst, Science **329**, 930 (2010).
[15] M. W. Klein, M. Wegener, N. Feth, and S. Linden, Opt. Express **15**, 5238 (2007); **16**, 8055 (2008).
[16] S. Kujala, B. Canfield, M. Kauranen, Y. Svirko, and J. Turunen, Opt. Express **16**, 17 196 (2008).
[17] M. Zdanowicz, S. Kujala, H. Husu, and M. Kauranen, New J. Phys. **13**, 023025 (2011).
[18] B. Canfield, H. Husu, J. Laukkanen, B. Bai, M. Kuittinen, J. Turunen, and M. Kauranen, Nano Lett. **7**, 1251 (2007).

[19] M. Klein, C. Enkrich, M. Wegener, and S. Linden, Science **313**, 502 (2006).
[20] C. Ciraci, E. Poutrina, M. Scalora, and D. R. Smith, Phys. Rev. B **85**, 201403 (2012).
[21] R. Czaplicki, M. Zdanowicz, K. Koskinen, J. Laukkanen, M. Kuittinen, and M. Kauranen, Opt. Express **19**, 26 866 (2011).
[22] H. Husu, R. Siikanen, J. Mäkitalo, J. Lehtolahti, J. Laukkanen, M. Kuittinen, and M. Kauranen, Nano Lett. **12**, 673 (2012).
[23] F. B. P. Niesler, N. Feth, S. Linden, and M. Wegener, Opt. Lett. **36**, 1533 (2011).
[24] M. Hentschel, T. Utikal, H. Giessen, and M. Lippitz, Nano Lett. **12**, 3778 (2012).
[25] T. Hanke, J. Cesar, V. Knittel, A. Trügler, U. Hohenester, A. Leitenstorfer, and R. Bratschitsch, Nano Lett. **12**, 992 (2012).
[26] H. Husu, J. Mäkitalo, R. Siikanen, G. Genty, H. Pietarinen, J. Lehtolahti, J. Laukkanen, M. Kuittinen, and M. Kauranen, Opt. Lett. **36**, 2375 (2011).
[27] S. Linden, F. B. P. Niesler, J. Förstner, Y. Grynko, T. Meier, and M. Wegener, Phys. Rev. Lett. **109**, 015502 (2012).
[28] H. Husu, J. Mäkitalo, J. Laukkanen, M. Kuittinen, and M. Kauranen, Opt. Express **18**, 16 601 (2010).
[29] F. J. García de Abajo, Rev. Mod. Phys. **79**, 1267 (2007).
[30] See Supplemental Material at http://link.aps.org/supplemental/10.1103/PhysRevLett.110.093902 for further details on the theoretical modeling.

Supplemental Material for "Enhancement of second-harmonic generation from metal nanoparticles by passive elements"

Robert Czaplicki[1], Hannu Husu[1,2], Roope Siikanen[1], Jouni Mäkitalo[1],
Janne Laukkanen[3], Joonas Lehtolahti[3], Markku Kuittinen[3] and Martti Kauranen[1]
[1] *Optics Laboratory, Department of Physics, Tampere University of Technology, P.O.Box 692, FI-33101 Tampere, Finland*
[2] *Centre for Metrology and Accreditation (MIKES), P. O. Box 9, FI-02151 Espoo, Finland*
[3] *Department of Physics and Mathematics, University of Eastern Finland, FI-80101 Joensuu, Finland*
(Dated: January 31, 2013)

As described in the main text of our Letter, the response of our particle array is modeled by treating the particles as electric point dipoles with anisotropic polarizabilities. It was shown that for such a system, the electric field at any given point is obtained by superposing the incident field with the field scattered by all the other dipoles. This was expressed by a direct summation, but in practice the summation is more convenient to include in periodic Green's function. Say that the periodicities in x- and y-directions are d_x and d_y as depicted in Fig. S1. A lattice translation

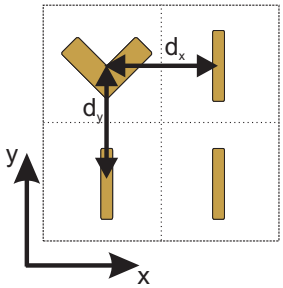

FIG. S1: Unit cell (sample **275L_xbar**) containing four particles with two distinct polarizabilities.

vector is defined as $\mathbf{t}_{nm} = nd_x\mathbf{x} + md_y\mathbf{y}$, where n and m are integers. The response of a periodic system can then be collected into a periodic Green's function g_p:

$$g_p(\mathbf{r},\mathbf{r}') = \sum_{n=-\infty}^{\infty}\sum_{m=-\infty}^{\infty}\frac{e^{ikR_{nm}}}{4\pi R_{nm}}, \tag{S1}$$

where $R_{nm} = |\mathbf{r}-\mathbf{r}'-\mathbf{t}_{nm}|$ and $\mathbf{r},\mathbf{r}'$ reside within the unit cell. The dyadic Green's function is given by $\overleftrightarrow{G}_p = (\mathbf{I} + k^{-2}\nabla\nabla)g_p$, similar to the non-periodic case. We also define the function $g_0(\mathbf{r},\mathbf{r}') = g_p(\mathbf{r},\mathbf{r}') - \exp(ik|\mathbf{r}-\mathbf{r}'|)/(4\pi|\mathbf{r}-\mathbf{r}'|)$, which is smooth at $\mathbf{r}=\mathbf{r}'$. That is, the field of the representative dipole in the array is excluded in g_0. The dyadic $\overleftrightarrow{G}_0$ is also defined as before.

If there are N different types of dipoles in the unit cell at locations $\mathbf{r}_n$ with polarizability tensors $\overleftrightarrow{\alpha}_n$, where $n = 1, 2, \ldots, N$, the coupled dipole model used in the Letter can be cast into the form

$$\mathbf{E}_m = \mathbf{E}_{0m} + k^2\overleftrightarrow{G}_0(\mathbf{r}_m,\mathbf{r}_m)\overleftrightarrow{\alpha}_m\mathbf{E}_m + k^2\sum_{\substack{n=1\\n\neq m}}^{N}\overleftrightarrow{G}_p(\mathbf{r}_m,\mathbf{r}_n)\overleftrightarrow{\alpha}_n\mathbf{E}_n, \tag{S2}$$

where $m = 1, 2, \ldots, N$. This linear system of equations may be written as $\mathrm{A}\mathbf{x} = \mathbf{b}$, where $\mathbf{x}$ consists of the components of $\mathbf{E}_n$ and $\mathbf{b}$ consists of the components of $\mathbf{E}_{0n}$.

In the special case of a simple periodic array of particles of one type only and x polarized field, i.e., $N = 1$ and $\mathbf{E}_1 = E\mathbf{x}$, we obtain

$$E = E_0 + k^2\overleftrightarrow{G}_{0xx}(0,0)\alpha E. \tag{S3}$$

The matrix A reduces into a scalar and the solution is explicit [1, 2].:

$$E = \frac{E_0}{1 - k^2\alpha\overleftrightarrow{G}_{0xx}(0,0)}. \tag{S4}$$

The series in Eq. S1 representations converge as $O(1/n)$ on the plane of the array. Thus for the numerical evaluation, the Ewald's method is utilized. This method leads to Gaussian convergence of g_p [3]. The differentials in the dyadic are evaluated with a finite-difference scheme.

The model in Eq. S2 is applied to the case illustrated in Fig. S1, where $N = 4$ and there are two distinct polarizabilities. The unit cell is square, i.e., $d_x = d_y$ as detailed in the Letter.

[1] F. J. García de Abajo, Rev. Mod. Phys. **79**, 1267 (2007).
[2] S. H. Mousavi, A. B. Khanikaev, B. Neuner, D. Y. Fozdar, T. D. Corrigan, P. W. Kolb, H. D. Drew, R. J. Phaneuf, A. Alù, and G. Shvets, Opt. Express **19**, 22142 (2011).
[3] G. Valerio, P. Baccarelli, P. Burghignoli, and A. Galli, IEEE Trans. Ant. Prop. **55**, 1630 (2007).